JCTC Journal of Chemical Theory and Computation

Article

pubs.acs.org/JCTC

Evaluating and Interpreting the Chemical Relevance of the Linear Response Kernel for Atoms

Zino Boisdenghien,*[,†] Christian Van Alsenoy,[‡] Frank De Proft,[†] and Paul Geerlings*[,†]

[†]Eenheid Algemene Chemie, Vrije Universiteit Brussel, Pleinlaan 2, 1050 Brussels, Belgium

[‡]Departement Chemie, Universiteit Antwerpen, Campus Drie Eiken, Universiteitsplein 1, 2610 Wilrijk, Belgium

ABSTRACT: Although a lot of work has been done on the chemical relevance of the atom-condensed linear response kernel χ_{AB} regarding inductive, mesomeric, and hyperconjugative effects as well as (anti)aromaticity of molecules, the same cannot be said about its not condensed form $\chi(\mathbf{r},\mathbf{r}')$. Using a single Slater determinant KS type ansatz involving second order perturbation theory, we set out to investigate the linear response kernel for a number of judiciously chosen closed (sub)shell atoms throughout the periodic table and its relevance, e.g., in relation to the shell structure and polarizability. The numerical results are to the best of our knowledge the first systematic study on this noncondensed linear response function, the results for He and Be being in line with earlier work by Savin. Different graphical representations of the kernel are presented and discussed. Moreover, a frontier orbital approach has been tested illustrating the sensitivity of the nonintegrated kernel to the nodal structure of the orbitals. As a test of our method, a numerical integration of the linear response kernel was performed, yielding an accuracy of 10^{-4}. We also compare calculated values of the polarizability tensor and their evolution throughout the periodic table to high-level values found in the literature.

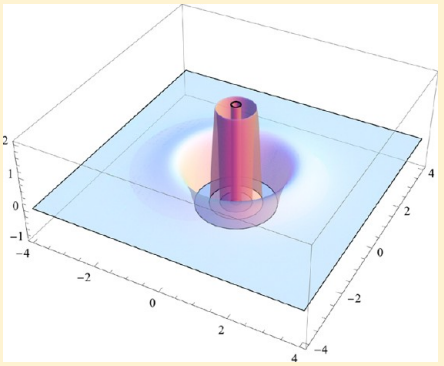

1. INTRODUCTION

The introduction of Density Functional Theory (DFT)[1−3] provided chemists with a framework in which quantum chemical calculations could be performed at an amazing quality/cost ratio. It however also prompted the development of Conceptual Density Functional Theory (CDFT)[2,4−6] or DFT chemical reactivity theory. This branch of DFT aims at providing a sound theoretical basis for chemical concepts which were already known but whose definitions were often rather vague. These concepts are described by reactivity indices or response functions which are defined as (functional) derivatives of the electronic energy E with respect to the external potential $v(\mathbf{r})$ and/or the number of electrons N. (Note that other reactivity indices without using derivatives are also possible, e.g. the description by Liu of the steric effect[7] and the description by Yang et al. of noncovalent interactions.[8]) The first and second derivatives of E with respect to N and $v(\mathbf{r})$ are now well documented (being the electronic chemical potential[9] $\mu = (\partial E/\partial N)_{v(\mathbf{r})}$, the electronic density $\rho(\mathbf{r}) = (\delta E/\delta v(\mathbf{r}))_N$, and the chemical hardness[10] $\eta = (\partial^2 E/\partial N^2)_{v(\mathbf{r})}$, as well as the mixed second order derivative, the Fukui function[11] $f(\mathbf{r}) = (\partial/\partial N(\delta E/\delta v(\mathbf{r}))_N)_{v(\mathbf{r}')}$). Even some of the third order derivatives received attention: the hyperhardness[12] $(\partial^3 E/\partial N^3)$ turned out to be chemically less important as opposed to one of the mixed $(v(\mathbf{r})/N)$ third order derivatives, the so-called dual descriptor[32] $(\partial f(\mathbf{r})/\partial N)_{v(\mathbf{r})}$ which provides a one shot picture of electrophilic and nucleophilic regions around a molecule. Both this quantity and the related initial hardness response[14] along a model reaction coordinate were central in the density-only retrieval of the Woodward−Hoffmann rules (see e.g. the recent review by some of the authors[15]).

Remarkably, the "diagonal" $(\delta^2 E/\delta v(\mathbf{r})\delta v(\mathbf{r}'))$ response function (or response kernel)[16] received relatively little attention, except from formal works by Senet,[17,18] Ayers and Parr,[19] Ayers,[20] and Cohen et al.[21] (For an overview of the mathematical properties of the linear response function, see Liu et al.[22]) Note that the link to its frequency dependent version in Time-Dependent DFT (TDDFT) has also been established.[2] It turned out until quite recently that its chemical information, obviously necessitating its numerical evaluation, received little attention with the exception of work by Baekelandt et al.,[23] Wang et al.[24] in highly approximate semiempirical schemes, and Morita and Kato[25,26] using coupled perturbed Hartree−Fock or Kohn−Sham equations. In very recent years, some of the current authors presented various methodologies to calculate the linear response function and were able to extract important chemical information from it,[27−32] based on the idea that $\chi(\mathbf{r},\mathbf{r}')$ can be written as $(\delta\rho(\mathbf{r})/\delta v(\mathbf{r}'))_N$, which represents the response of the electronic density of e.g. a molecular system at point $\mathbf{r}$ when its external potential is perturbed at a point $\mathbf{r}'$.

Basic chemical concepts such as inductive, mesomeric and hyperconjugative effects, aromaticity, and antiaromaticity could be retrieved in a series of papers concentrating on molecules where due to the nature of the kernel a condensation scheme of $\chi(\mathbf{r},\mathbf{r}')$ to an atom−atom matrix χ_{AB}[33−35] was invariably chosen. It is our goal in this paper, however, to study the linear

Received: October 5, 2012
Published: January 4, 2013

response function rather than the linear response matrix, i.e., avoiding any condensation. For this purpose, our attention is focused on atoms. To the best of our knowledge, there is only one publication in which numerical values for the linear response kernel calculated on atoms are reported.[36] The results in that pioneering work are restricted to very light atoms and, e.g., the evolution along the periodic table and the chemical relevance of the results were not discussed, nor is the significance of the sign of the various regions of the linear response kernel and its relation to other concepts such as the polarizability. We therefore embarked on a study of the linear response function for a series of atoms with a 1_S ground state, judiciously chosen in the periodic table, in order to retrieve, just as for the matrix condensed form for molecules, chemical or physical relevance from this higher resolution picture. We will focus on the noble gases helium through krypton and the alkaline earth metals beryllium through calcium, as well as a couple of isoelectronic series: F^-, Ne, Na^+, and Mg^{2+} and Cl^-, Ar, K^+, and Ca^{2+}. These atoms are chosen for the sake of their filled subshell structure immediately leading to spherical symmetry (vide infra). Note that the work done in this paper also fits nicely in the extensive literature on the shell structure of atoms.[37]

2. THEORETICAL BACKGROUND

The basic equation in CDFT or chemical reactivity theory is the Taylor expansion of the energy as a functional of N (the number of electrons) and $v(\mathbf{r})$ (the external potential)[2,6]

$$\begin{aligned} &E[N_0 + \Delta N, v_0(\mathbf{r}) + \Delta v(\mathbf{r})] - E[N_0, v_0(\mathbf{r})] \\ &= \left(\frac{\partial E}{\partial N}\right)_{v(\mathbf{r})} \Delta N + \frac{1}{2}\left(\frac{\partial^2 E}{\partial N^2}\right)_{v(\mathbf{r})} (\Delta N)^2 + \ldots \\ &+ \int \mathrm{d}\mathbf{r}\left(\frac{\delta E}{\delta v(\mathbf{r})}\right)_N \Delta v(\mathbf{r}) \\ &+ \Delta N \int \mathrm{d}\mathbf{r}\left(\frac{\partial}{\partial N}\left(\frac{\delta E}{\delta v(\mathbf{r})}\right)_N\right)_{v(\mathbf{r})} \Delta v(\mathbf{r}) + \ldots \\ &+ \frac{1}{2}\int \mathrm{d}\mathbf{r}\,\mathrm{d}\mathbf{r}'\left(\frac{\delta^2 E}{\delta v(\mathbf{r})\delta v(\mathbf{r}')}\right)_N \Delta v(\mathbf{r})\Delta v(\mathbf{r}') + \ldots \end{aligned} \tag{1}$$

where now the different response functions can be identified. For an analysis of the convergence and formal properties of this series, see Ayers et al.[38] The kernel in the last line of eq 1 defines the linear response kernel, which can be expressed as

$$\chi(\mathbf{r}, \mathbf{r}') = \left(\frac{\delta^2 E}{\delta v(\mathbf{r})\delta v(\mathbf{r}')}\right)_N = \left(\frac{\delta \rho(\mathbf{r})}{\delta v(\mathbf{r}')}\right)_N \tag{2}$$

This gives us a useful interpretation of the linear response kernel as the change in electron density in a point $\mathbf{r}$ in response to a perturbation of the external potential in a point $\mathbf{r}'$.

Explicit numerical differentiation techniques of the energy functional with respect to the external potential, leading in the limit to exact values, have been presented by some of the present authors but turned out to be extremely time-consuming.[14,27,30,39] For closed shell systems described by a single Slater determinant, we can use second order perturbation theory to approximate the linear response kernel in terms of molecular orbitals[2,20,40]

$$\chi(\mathbf{r}, \mathbf{r}') \approx 4 \sum_{i,a} \frac{\psi_i^*(\mathbf{r})\psi_a(\mathbf{r})\psi_a^*(\mathbf{r}')\psi_i(\mathbf{r}')}{\varepsilon_i - \varepsilon_a} \tag{3}$$

where i runs over occupied orbitals and a runs over unoccupied orbitals. This expression for the linear response kernel can be derived from second-order perturbation theory given two approximations: first, one must assume the so-called frozen orbital approximation, in which excited states are constructed by substituting unoccupied molecular spin orbitals for occupied ones in the single Slater determinant used to describe the molecular wave function without relaxation of this new set of spin orbitals. Second, the energy differences between excited states and the ground state must be replaced by differences in orbital energy. Note that these assumptions are exactly applicable to the Kohn−Sham (KS) noninteracting reference system.[3] In other words, we can interpret eq 3 as the exact functional derivative of the electron density with respect to the KS potential $v_{KS}(\mathbf{r})$.[18,20]

It can easily be shown analytically that[22]

$$\int \mathrm{d}\mathbf{r}'\chi(\mathbf{r}, \mathbf{r}') = 0 \tag{4}$$

and that the polarization tensor can be expressed in terms of an integral over the linear response kernel as[2,40]

$$\alpha_{ij} = -\int \mathrm{d}\mathbf{r}\,\mathrm{d}\mathbf{r}'\, r_i\chi(\mathbf{r}, \mathbf{r}')r_j' \quad (i, j = x, y, z) \tag{5}$$

where r_i denotes the ith component of the vector $\mathbf{r}$. We shall use eq 4 as a test for our calculated values of the linear response kernel and compare the calculated values of α_{ii} using eq 5 to values found in the literature—serving as a secondary test.

The importance of this connection between the polarization tensor α_{ij} and the linear response kernel $\chi(\mathbf{r},\mathbf{r}')$ among other aspects lies in the fact that if we manage to find simple and accurate expressions for $\chi(\mathbf{r},\mathbf{r}') = (\delta\rho(\mathbf{r})/\delta v(\mathbf{r}'))_N$, e.g., in wave function free theories, we can easily calculate the polarizability tensor from it by (numerical) integration.

3. METHODOLOGY

We will use eq 3[40] to calculate the linear response kernel. Specifically, in the case of a closed shell system containing N_0 electrons in the KS ansatz

$$\chi(\mathbf{r}, \mathbf{r}') = 4 \sum_{i=1}^{N_0/2} \sum_{a=(N_0/2)+1}^{\infty} \frac{\psi_i^*(\mathbf{r})\psi_a(\mathbf{r})\psi_a^*(\mathbf{r}')\psi_i(\mathbf{r}')}{\varepsilon_i - \varepsilon_a} \tag{6}$$

This expression allows for a straightforward computational evaluation of the linear response kernel. The orbitals were obtained using a 6-311+G*[41] and an aug-cc-pVTZ[42−44] basis set at the PBE[45] level of theory and using the Stock software.[46] Orbitals were calculated with Gaussian 09.[47]

For the integrations, eqs 4 and 5, grids were used as in regular SCF calculations. In our case, these consist of a combination of Euler-MacLaurin[48] and Lebedev[49] grids for the radial and angular integration, respectively, as proposed by Gill et al.[50]

4. RESULTS AND DISCUSSION

4.1. Light Elements. We shall start by comparing our computed results for the linear response kernel with the results found in ref 36 as far as possible. The plots in Figure 1 (as well as similar plots throughout this paper) show the "radial distribution" of the linear response kernel in the case of a

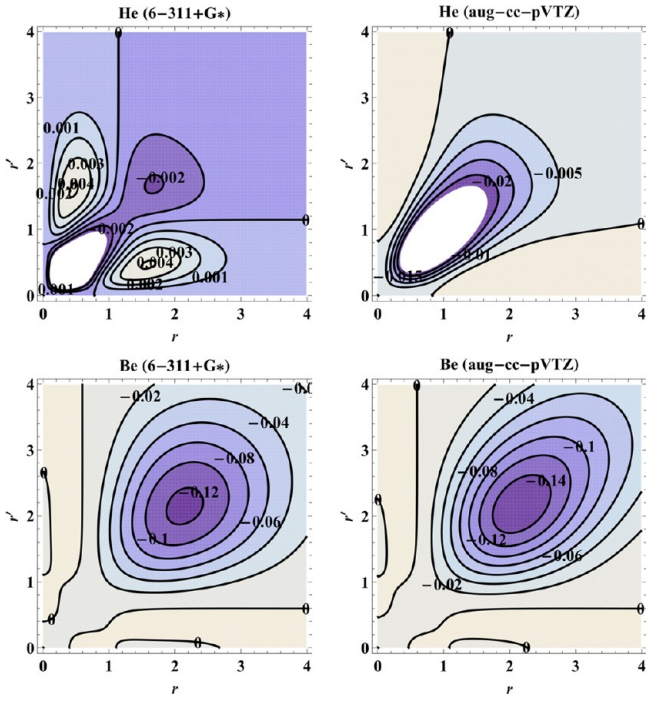

Figure 1. Contour plots for the radial distribution of the linear response kernel $r^2\chi(r,r')r'^2$ for He and Be, calculated with both a 6-311+G* basis set and an aug-cc-pVTZ basis set.

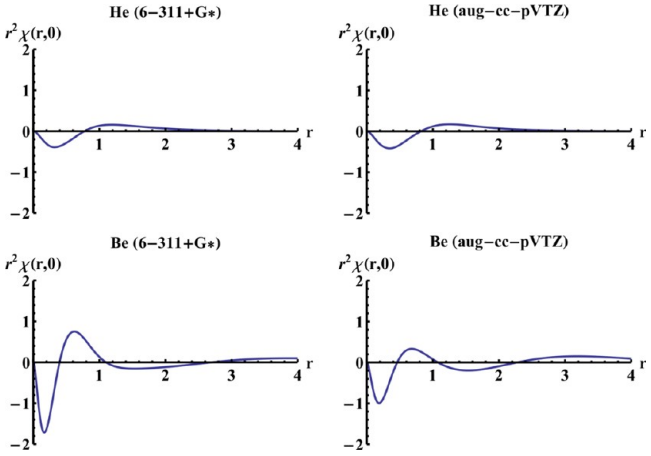

Figure 2. One-dimensional section of the radial distribution of the linear response kernel along the r axis, $r^2\chi(r,\mathbf{0})$, for He and Be, calculated with both a 6-311+G* basis set and an aug-cc-pVTZ basis set.

spherical potential perturbation, $r^2\chi(r,r')r'^2$, for helium and beryllium with the nucleus at the origin. Note that the quantities on the axes of these plots are not Cartesian coordinates but the distance to the origin/nucleus for $\mathbf{r}$ and $\mathbf{r}'$ which are the coordinates of the points where we investigate the change in electron density $\delta\rho(\mathbf{r})$ for a perturbation $\delta v(\mathbf{r}')$, respectively. These plots are directly comparable to the corresponding plots in Figure 2 in the work by Savin et al.[36] As also mentioned there, we can clearly see two distinct regions arise, one negative and one positive, in the plots for helium. These get duplicated when moving to beryllium, an effect which can be attributed to the shell structure.

In order to simplify the interpretation of these plots, however, we turn to one-dimensional versions of the previously

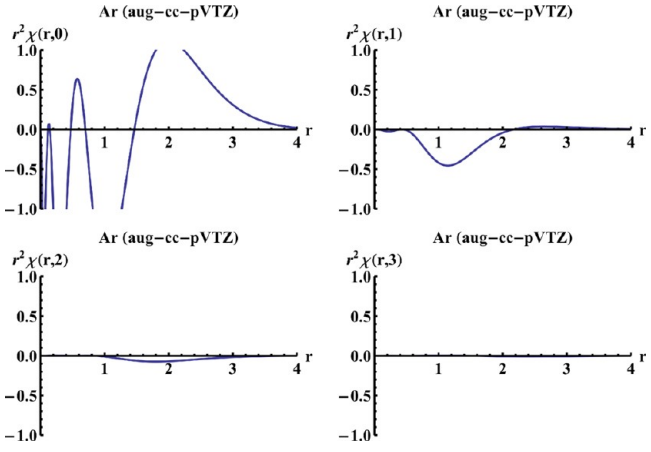

Figure 3. One-dimensional sections of the radial distribution of the linear response kernel along the r axis, $r^2\chi(r,r')$, for argon and multiple fixed values for r'. These plots were calculated using an aug-cc-pVTZ basis set.

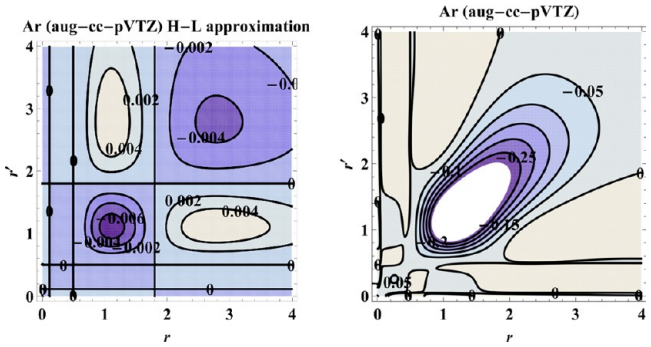

Figure 4. Contour plot for the radial distribution of the linear response kernel $r^2\chi(r,r')r'^2$ for Ar, calculated with the aug-cc-pVTZ basis set using the HOMO−LUMO approximation. This plot is compared to the contour plot for $r^2\chi(r,r')r'^2$ using the full summation in eq 6, still for Ar and using an aug-cc-pVTZ basis set.

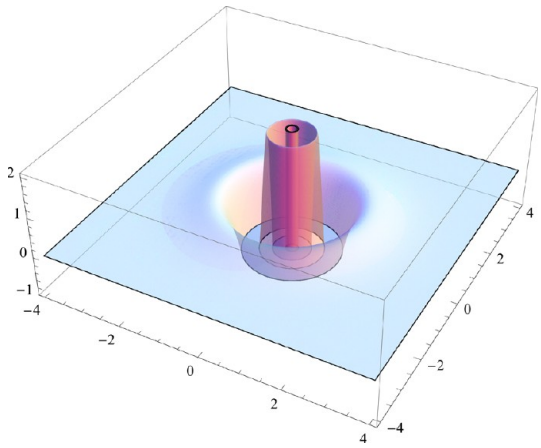

Figure 5. Plot for the linear response kernel $\chi(\mathbf{r},\mathbf{0})$ for Ar where the perturbation is placed in the origin and $\mathbf{r}$ is varied over the (x,y) plane.

mentioned contour plots. These plots, shown in Figure 2 for helium and beryllium, show the function $r^2\chi(r,r')$ for a fixed value for r', which we have chosen to be the origin. In other words, these one-dimensional plots are a cross section of the full contour plots along the r axis. Note that there are no

dx.doi.org/10.1021/ct300861r | J. Chem. Theory Comput. 2013, 9, 1007−1015

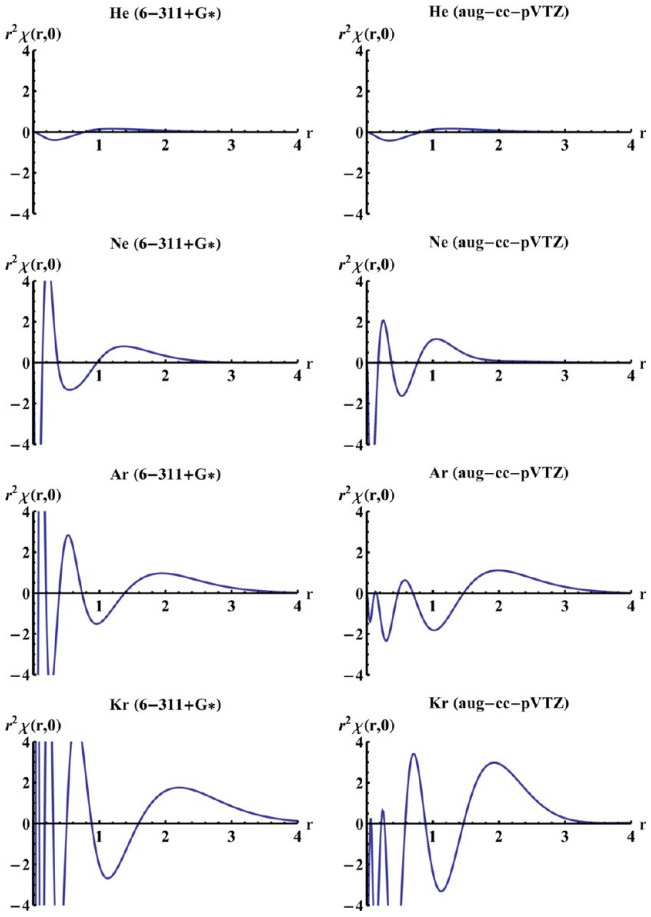

Figure 6. One-dimensional sections of the radial distribution of the linear response kernel along the r axis, $r^2\chi(r,\mathbf{0})$, for the first four noble gases, calculated with both a 6-311+G* basis set and an aug-cc-pVTZ basis set.

corresponding one-dimensional plots in the work by Savin et al.[36] to which to compare these plots.

We note that the core region of the linear response kernel (closest to the nucleus) is negative. In the absence of external fields, the external potential $v(\mathbf{r}_i)$ can be written as

$$v(\mathbf{r}_i) = -\sum_{A=1}^{N_{\text{nucl}}} \frac{Z_A}{|\mathbf{r}_i - \mathbf{r}_A|} \tag{7}$$

with $V_{\text{ne}} = \sum_{i=1}^{N} v(\mathbf{r}_i)$ the total electron−nucleus interaction operator. In this expression, N and N_{nucl} represent the number of electrons and nuclei, respectively, where in the case of atoms, N_{nucl} evidently equals one. Furthermore, $\mathbf{r}_i$ represents the position vector of electron i, $\mathbf{r}_A$ the nuclear coordinates, and Z_A the charge of the Ath nucleus. Due to the minus sign, $v(\mathbf{r})$ represents an attractive potential. If we then assume a positive perturbation $\delta v(\mathbf{r})$, the external potential becomes less negative, resulting in a smaller attraction due to the nucleus and thus an electron density depletion in the vicinity of the nucleus.

More specifically, we know that at constant number of electrons N

$$\Delta\rho(\mathbf{r}) = \int d\mathbf{r}' \left(\frac{\delta\rho(\mathbf{r})}{\delta v(\mathbf{r}')}\right)_N \delta v(\mathbf{r}') = \int d\mathbf{r}' \chi(\mathbf{r}, \mathbf{r}')\delta v(\mathbf{r}') \tag{8}$$

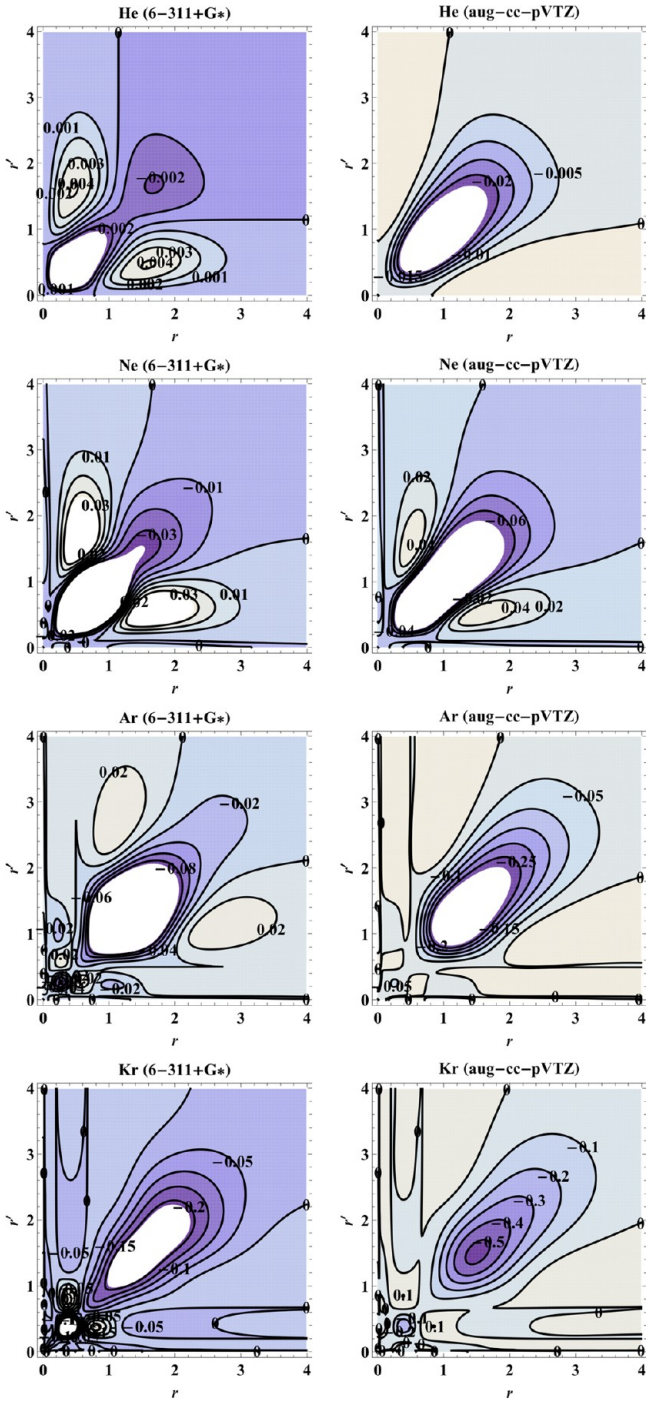

Figure 7. Contour plots for $r^2\chi(r,r')r'^2$ for the first four noble gases, calculated with a 6-311+G* basis set as well as an aug-cc-pVTZ basis set.

Let us assume, for the sake of interpretation, a point like perturbation[51] of the external potential, $\delta v(\mathbf{r}) = A\delta(\mathbf{r} - \mathbf{0})$, where we assume A to be a positive real constant. This implies

$$\Delta\rho(\mathbf{r}) = A\chi(\mathbf{r}, \mathbf{0}) \tag{9}$$

From this, we see that for a positive perturbation $\delta v(\mathbf{r})$, negative regions in the linear response kernel imply a drop in electron density corresponding to a negative region in the one-dimensional plot close to the nucleus, which is accompanied, at a longer distance, by a positive region in view of the conservation of the number of electrons. Note that this is

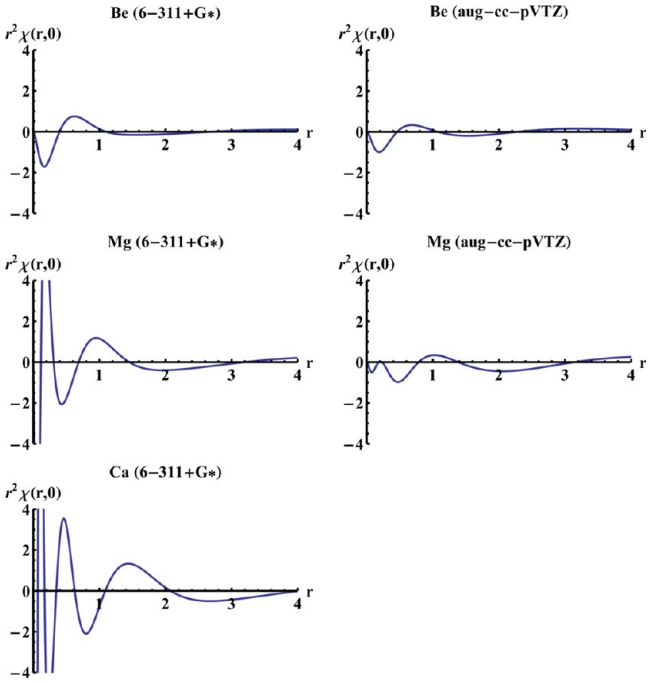

Figure 8. One-dimensional plots for $r^2\chi(r,\mathbf{0})$ for the first three IIa elements, calculated with a 6-311+G* basis set as well as an aug-cc-pVTZ basis set. Note that there is no aug-cc-pVTZ basis set available for Ca in Gaussian 09.

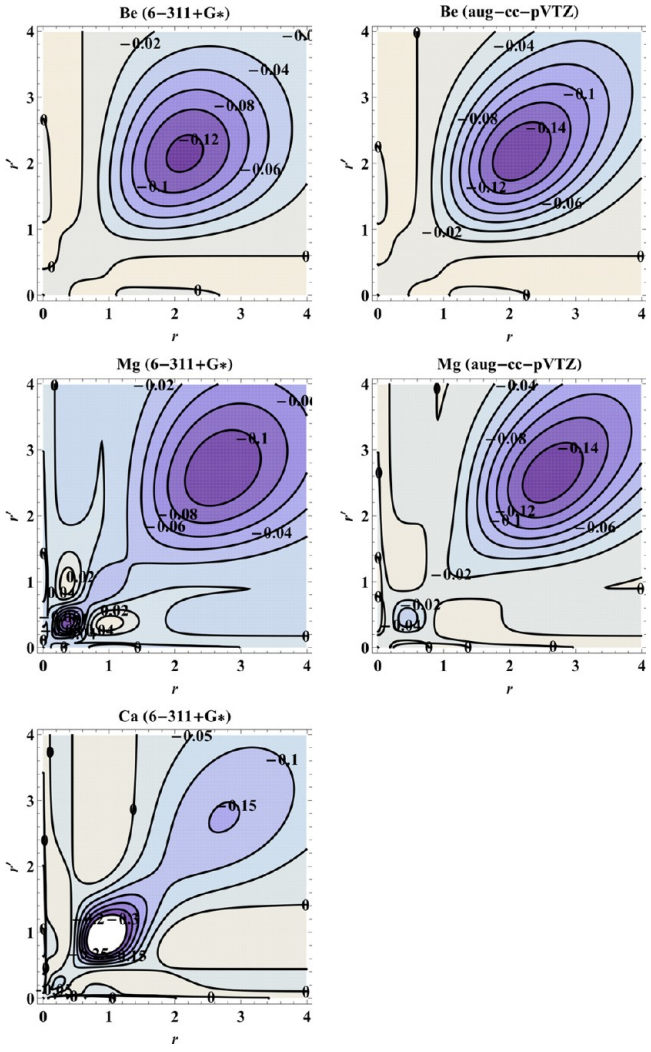

Figure 9. Contour plots for $r^2\chi(r,r')r'^2$ for the first three IIa elements, calculated with a 6-311+G* basis set as well as an aug-cc-pVTZ basis set. Again, note that there is no aug-cc-pVTZ basis set available for Ca in Gaussian 09.

consistent with eq 4. Returning to the two-dimensional plots in Figure 1, we recognize in the plot for helium in the regions close to the r and r' axes the alternation of negative and positive regions from the one-dimensional plot, the perturbation being still close to the nucleus. If we move to the central part of the plot, the perturbation (say at r) is now far from the nucleus and, say in the case of a less negative $v(r)$, ($\Delta v(r) > 0$) incites an electron depletion in the tail of the electron distribution at r' ($\Delta\rho(r') < 0$) leading to the dominantly negative part of the plot for larger r and r'. We must also mention that there are strong differences between both plots for helium. These differences, which are not qualitative in nature, can be attributed to the differences in the basis sets. Passing to the case of beryllium, one sees that the nodal structure of the one-dimensional plots is now translated into a more complex figure, especially at low r and r'.

When passing from helium to beryllium, the sequence of negative and positive regions near the nucleus is the same, but the curve shows further nodal structure which can be attributed to the shell structure.

4.2. General Remarks. As mentioned above, the one-dimensional plots in Figure 2 are cross-sections of the two-dimensional contour plots in Figure 1 along the horizontal axis. We can also take cross-sections along other horizontal lines at some value r' in these contour plots, corresponding to similar one-dimensional plots which plot the change in electron density for a point at a distance r' from the nucleus. Such plots are shown in Figure 3

We clearly see a reduced effect of the perturbation on the density. This implies that the effect of a perturbation $\delta v(\mathbf{r}')$ on the electronic density in $\mathbf{r}$ is highest when the perturbation is placed close to the nucleus.

To investigate which orbitals dominate the linear response kernel through eq 3 we used a frontier orbital approximation retaining only the HOMO and LUMO orbitals in the summation (taking into account possible degeneracy of these orbitals). The resulting contour plot for argon is shown in Figure 4, where it is compared to the corresponding contour plot for argon obtained with eq 6, which will be further discussed in section 4.3. Note that since in this case the HOMO is a p-orbital which contains a node in the origin, when either $\mathbf{r}$ or $\mathbf{r}'$ is zero, the linear response kernel is zero along the axes in this approximation. This will happen whenever either the HOMO or LUMO contains a node in the origin. This results in a figure which is highly deformed as compared to the full summation expression. This shows the extreme sensitivity of the nonintegrated kernel to the nodal structure of the orbitals and warns for a frontier MO approach.

Finally, as remarked above, the axes of the two-dimensional contour plots do not label any Cartesian coordinates but rather distances to the origin. These contour plots provide us with insight in the radial distribution of the linear response kernel. We can however represent the response function in a more appealing way by placing a perturbation in the origin (remember that this is where the nucleus is located) and

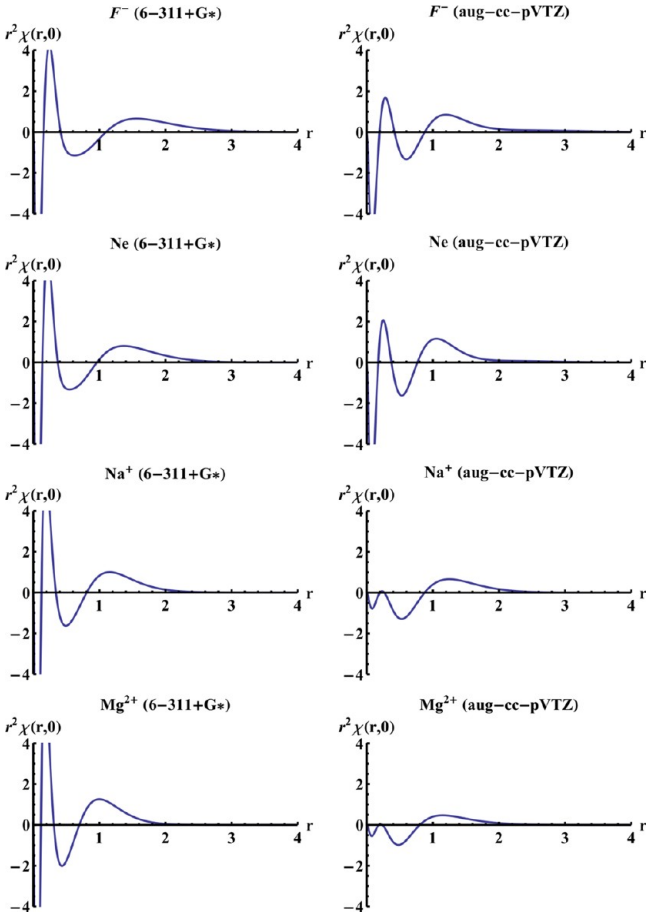

Figure 10. One-dimensional plots for $r^2\chi(r,\mathbf{0})$ for the Ne isoelectronic series, calculated with a 6-311+G* basis set as well as an aug-cc-pVTZ basis set.

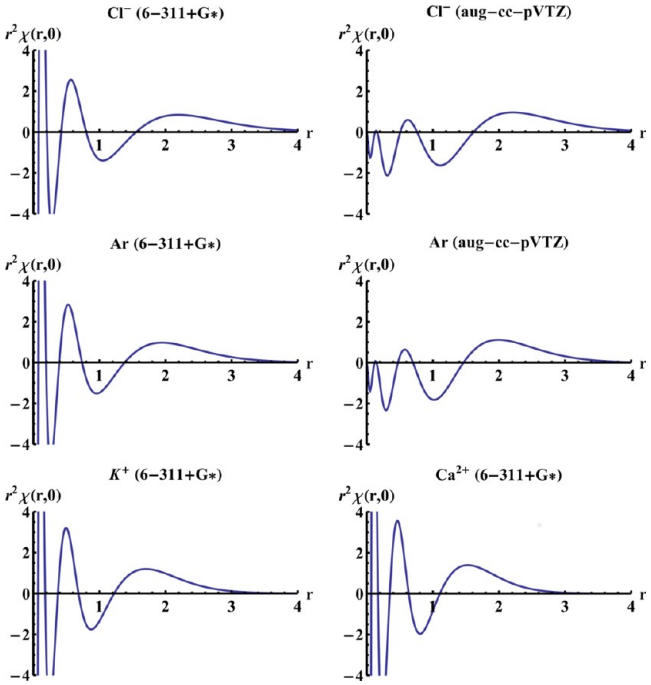

Figure 11. One-dimensional plots for $r^2\chi(r,\mathbf{0})$ for the Ar isoelectronic series, calculated with a 6-311+G* basis set as well as an aug-cc-pVTZ basis set. Note that as for Ca, there is no aug-cc-pVTZ basis set available for K^+ and Ca^{2+}.

scanning the response of the electronic density in the (x,y) plane. This is shown in Figure 5

In this plot, the alternation in sign of the response function, already emerging from the previous plots, is retrieved together with the diminishing effect of the perturbation for increasing distance to the origin. The alternating pattern of peaks and valleys is—as mentioned before for the contour plots—related to the shell structure.

4.3. Systematic Extension along the Periodic Table. We shall now make our way throughout the periodic table to study some systematics in a few selected series of atoms and ions.

4.3.1. Noble Gases. Starting again from the evolution in the one-dimensional plots (Figure 6), we see that the curve starts with a negative region close to the nucleus (cf. helium) followed by a positive one and a number of oscillations reflecting the shell structure. This is comparable with e.g. the observations of the average local electrostatic potential function,[52−54] $(V(r)/\rho(r))$.

Extending the plots in Figure 6 to the two-dimensional case yields Figure 7, showing the contour plots for $r^2\chi(r,r')r'^2$ for the first four noble gases.

In the regions for small r and r', more oscillations pop up whereas the central region for larger r and r' remains negative and spreads out upon increasing atomic number of the noble gas. As eq 5 shows, the linear response kernel is related to the polarizability of the atom, and the fact that the linear response kernel extends further away from the nucleus is intimately related to the increasing polarizability when going down in a given column in the periodic table.[55]

4.3.2. IIa Elements. Figures 8 and 9 show the results for the first three IIa elements, i.e., Be, Mg, and Ca. We see the same evolution as with the noble gases—the linear response kernel gets more extended when going down in the periodic table and we see a doubling of regions reflecting the shell structure—but the linear response kernel is initially more extended than was the case for noble gases, reflecting the fact that IIa elements are more polarizable than noble gases, in line with the trend of decreasing polarizability when going from left to right in the periodic table.[55]

4.3.3. Isoelectronic Series. In Figures 10−13, the results for the Ne and Ar isoelectronic series are shown: the number of regions does not change in any of these series since the number of shells does not change. What does change is the extent of the linear response kernel around the nucleus related to the extent of the system and its polarizability: an anion is more polarizable because its electrons are more loosely bound to the nucleus and its valence electrons more susceptible to external potential perturbations. Moving to the cations shows a more contracted linear response kernel, reflecting the fact that when passing from neutral atoms to cations these systems become less and less polarizable with neutral atoms lying in between cations and anions.

4.4. Polarizability. The values for the α_{xx} element of the polarizability tensor were calculated using eq 5. In view of the spherical symmetry of the system, this value is also equal to the overall polarizability of the system. Our values are given in Table 1 along with high-level calculated values taken from Mitroy et al.[56] where available (we used values calculated with the relativistic random-phase approximation method where possible, the CI method otherwise). It is evident that our

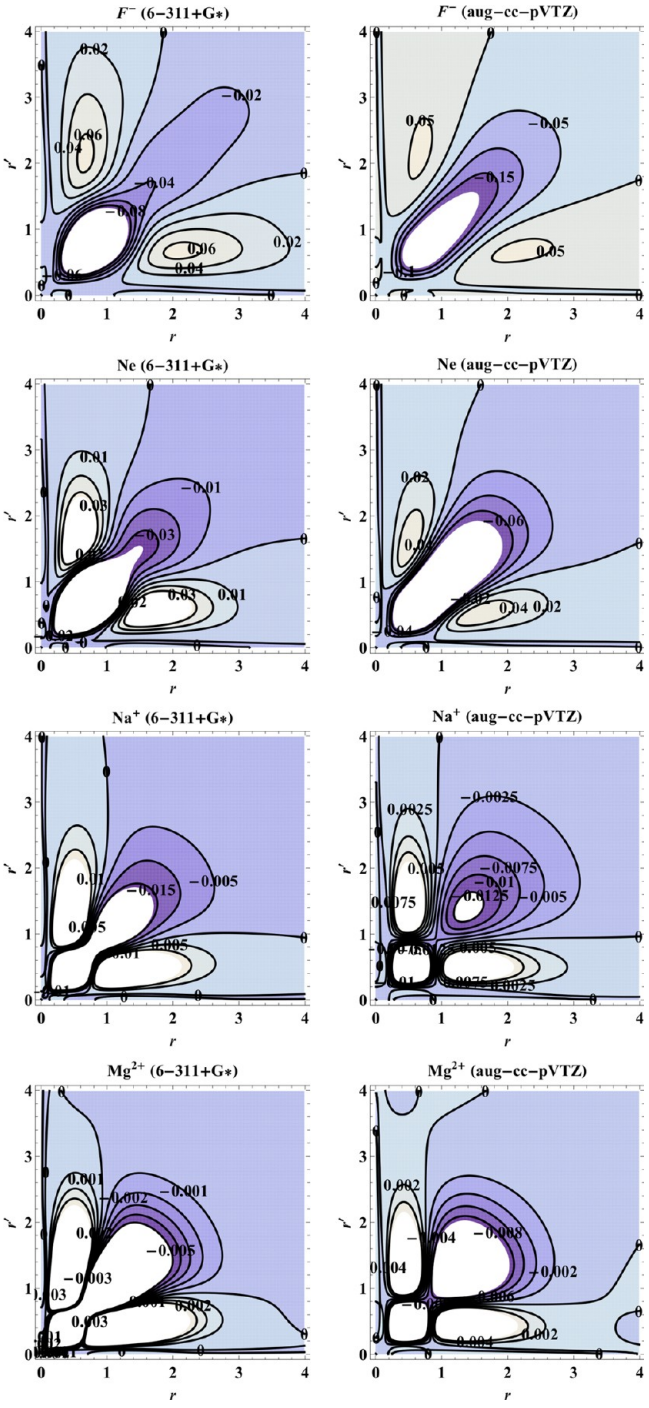

Figure 12. Contour plots for $r^2\chi(r,r')r'^2$ for the Ne isoelectronic series, calculated with a 6-311+G* basis set as well as an aug-cc-pVTZ basis set.

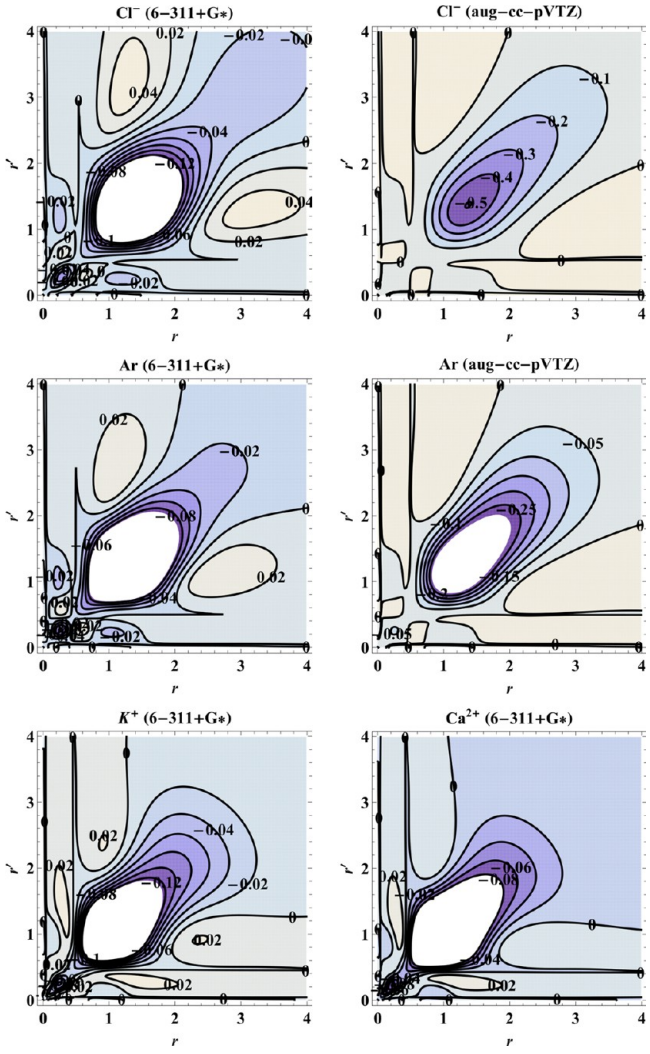

Figure 13. Contour plots for $r^2\chi(r,r')r'^2$ for the Ar isoelectronic series, calculated with a 6-311+G* basis set as well as an aug-cc-pVTZ basis set. Note that as for Ca, there is no aug-cc-pVTZ basis set available for K^+ and Ca^{2+}.

calculated values are expected to be not of comparable accuracy to these high level calculations in view of the still highly approximate nature for the evaluation of $\chi(\mathbf{r},\mathbf{r}')$, eq 3. Nevertheless, trends are representative.

If we look at the high-level values for the noble gases, we see that the ratio between these high-level values for α_{xx} and ours varies between 1.3 and 1.7. When we look at the ratios between the values of He to Ne, Ne to Ar, and Kr to Xe, our values of 1.8, 5.5, and 1.6 are close to the high-level values of 1.8, 4.5, and 1.5, especially in view of the still highly approximate expression for the linear response kernel. Going through the periodic table, the ratios of the high-level α_{xx} values for the IIa elements are 1.9 and 2.2 for Be to Mg and Mg to Ca, respectively, compared

Table 1. Calculated Values for α_{xx} Using eq 5 for Both the 6-311+G* Basis Set and the aug-cc-pVTZ Basis Set[a]

element	6-311+G*	aug-cc-pVTZ	Mitroy et al.	method
He	n/a	1.688	1.322	RRPA
Be	77.953	77.940	37.807	CI
F^-	5.356	11.526	n/a	n/a
Ne	1.196	3.070	2.38	RRPA
Na^+	0.619	0.523	0.9457	RRPA
Mg^{2+}	0.182	0.296	0.4698	RRPA
Mg	124.761	124.597	70.9	CI
Cl^-	19.335	44.313	n/a	n/a
Ar	6.872	16.918	10.77	RRPA
K^+	8.349	n/a	5.457	RRPA
Ca^{2+}	4.866	n/a	3.254	RRPA
Ca	289.878	n/a	156	CI
Kr	17.227	27.199	16.47	RRPA

[a]When available, we also include high-level reference values taken from Mitroy et al.[56]

dx.doi.org/10.1021/ct300861r | J. Chem. Theory Comput. 2013, 9, 1007−1015

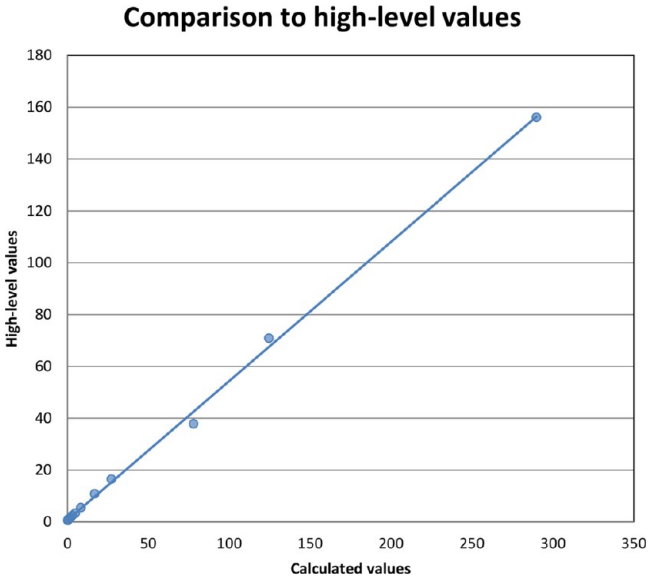

Figure 14. Scatter plot comparing our calculated polarizability values (on the horizontal axis) to high-level values.[56]

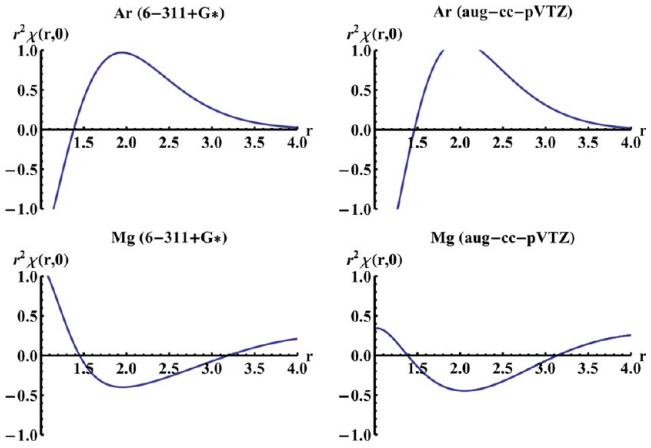

Figure 15. Comparison of the plots for $r^2\chi(r,0)$ for Mg and Ar, calculated with a 6-311+G* basis set as well as an aug-cc-pVTZ basis set. Note that for magnesium, the plot does not decrease to zero as fast as for argon.

to 1.6 and 2.3 for the calculated values (using the 6-311+G* basis set). For the Ne isoelectronic series, the ratios of our calculated values are 0.2, 0.5, and 0.3, whereas for the high-level values, these ratios are 0.4 and 0.5 for Ne to Na^+ and Na^+ to Mg^{2+}, respectively. Note that there were no values available for F^-. For the Ar isoelectronic series, finally, our calculated values yielded 0.4, 1.2, and 0.6 for the ratios Cl^- to Ar, Ar to K^+, and K^+ to Ca^{2+}, respectively (using the 6-311+G* basis set). Again, there were no high-level values available for Cl^-, but the ratios for Ar to K^+ and K^+ to Ca^{2+} were 0.5 and 0.6.

Figure 14 shows the comparison of our calculated values to the high-level values. It is clear from this figure that our calculated values capture the trends governing α throughout the periodic table quite well.

We note that for IIa elements the difference between our calculated values and the referenced values is large. The reason for these large deviations is related to the extent of the linear response kernel. In Figure 15, we compare the plots for $r^2\chi(r,0)$ for Mg and Ar. We notice that the plot for Ar decreases to zero more rapidly than the one for Mg. This is a feature we find for all IIa elements. This slower decrease to zero introduces a computational inaccuracy in the numerical integration causing the deviating values. Note that we have used eq 4 as a validation protocol for our procedure by integrating the linear response kernel over $\mathbf{r}'$ and repeating this integration for all $\mathbf{r}$ in the grid. By fine tweaking the integration grids, we can show that the linear response kernel for all elements integrates to zero with a maximum deviation (in absolute value) of 10^{-4}, showing that our procedure is indeed numerically sound.

5. CONCLUSION

A simple and systematic procedure for the evaluation of the noncondensed linear response function is presented for application to closed shell atoms throughout the periodic table. The numerical results are to the best of our knowledge the first systematic study reported in the literature on the noncondensed linear response function. The results for $\chi(r,r')$ for helium and beryllium are in line with earlier results by Savin.[36] The different types of plots reveal the relation between the linear response kernel and the shell structure. It is also shown how a perturbation further away from the nucleus has less influence on the electronic density (eq 3). Finally, prudence is also called for the use of a frontier MO approximation due to the sensitivity of the nonintegrated kernel to the nodal structure of these frontier orbitals.

All in all, the present paper shows that besides the chemical relevance present in the condensed linear response function under the form of information about inductive, mesomeric, hyperconjugative effects and aromaticity and antiaromaticity as shown in refs 27−32, its physical relevance nicely shows up in its noncondensed form in the simplest systems as closed (sub)shell atoms through various types of plots and in an integrated form through the polarizability. Further work on open shell atoms is in progress.

AUTHOR INFORMATION

Corresponding Author

*E-mail: zboisden@vub.ac.be; pgeerlin@vub.ac.be.

Notes

The authors declare no competing financial interest.

REFERENCES

(1) Hohenberg, P.; Kohn, W. *Phys. Rev.* **1964**, *136*, B864−B871.
(2) Parr, R. G.; Yang,W. *Density-Functional Theory of Atoms and Molecules; International Series of Monographs on Chemistry*; Oxford University Press: New York, 1989.
(3) Kohn, W.; Sham, L. J. *Phys. Rev.* **1965**, *140*, A1133−A1138.
(4) Liu, S. B. *Acta Phys.—Chim. Sin.* **2009**, *25*, 590−600.
(5) Johnson, P. A.; Bartolotti, L. J.; Ayers, P. W.; Fievez, T.; Geerlings, P. In *Charge Density and Chemical Reactions: A Unified View from Conceptual DFT*; Gatti, C., Macchi, P., Eds.; Springer: New York, 2012; pp 715−764.
(6) (a) Geerlings, P.; De Proft, F.; Langenaeker, W. *Chem. Rev.* **2003**, *103*, 1793−1874. (b) Chermette, H. *J. Comput. Chem.* **1999**, *20*, 129−154.
(7) Liu, S. *J. Chem. Phys.* **2007**, *126*, 244103.
(8) Johnson, E. R.; Keinan, S.; Mori-Sánchez, P.; Contreras-García, J.; Cohen, A. J.; Yang, W. *J. Am. Chem. Soc.* **2010**, *132*, 6498−6506.
(9) Donnelly, R. A.; Parr, R. G. *J. Chem. Phys.* **1978**, *69*, 4431−4439.
(10) Parr, R. G.; Pearson, R. G. *J. Am. Chem. Soc.* **1983**, *105*, 7512−7516.
(11) Parr, R. G.; Yang, W. *J. Am. Chem. Soc.* **1984**, *106*, 4049−4050.
(12) Fuentealba, P.; Parr, R. G. *J. Chem. Phys.* **1991**, *94*, 5559−5564.

(13) Morell, C.; Grand, A.; Toro-Labbé, A. *J. Phys. Chem. A* **2005**, *109*, 205−212.
(14) Ayers, P. W.; De Proft, F.; Borgoo, A.; Geerlings, P. *J. Chem. Phys.* **2007**, *126*, 224107.
(15) Geerlings, P.; Ayers, P. W.; Toro-Labbé, A.; Chattaraj, P. K.; De Proft, F. *Acc. Chem. Res.* **2012**, *45*, 683−695.
(16) Berkowitz, M.; Parr, R. G. *J. Chem. Phys.* **1988**, *88*, 2554−2557.
(17) Senet, P. *J. Chem. Phys.* **1996**, *105*, 6471−6489.
(18) Senet, P. *J. Chem. Phys.* **1997**, *107*, 2516−2524.
(19) Ayers, P. W.; Parr, R. G. *J. Am. Chem. Soc.* **2001**, *123*, 2007−2017.
(20) Ayers, P. W. *Theor. Chem. Acc.* **2001**, *106*, 271−279.
(21) Cohen, M. H.; Ganduglia-Pirovano, M. V.; Kudrnovský, J. *J. Chem. Phys.* **1995**, *103*, 3543−3551.
(22) Liu, S.; Li, T.; Ayers, P. W. *J. Chem. Phys.* **2009**, *131*, 114106.
(23) Baekelandt, B. G.; Mortier, W. J.; Lievens, J. L.; Schoonheydt, R. A. *J. Am. Chem. Soc.* **1991**, *113*, 6730−6734.
(24) Wang, C.-S.; Zhao, D.-X.; Yang, Z.-Z. *Chem. Phys. Lett.* **2000**, *330*, 132−138.
(25) Morita, A.; Kato, S. *J. Phys. Chem. A* **2002**, *106*, 3909−3916.
(26) Morita, A.; Kato, S. *J. Am. Chem. Soc.* **1997**, *119*, 4021−4032.
(27) Sablon, N.; De Proft, F.; Ayers, P. W.; Geerlings, P. *J. Chem. Phys.* **2007**, *126*, 224108.
(28) Sablon, N.; De Proft, F.; Geerlings, P. *J. Phys. Chem. Lett.* **2010**, *1*, 1228−1234.
(29) Sablon, N.; De Proft, F.; Geerlings, P. *Chem. Phys. Lett.* **2010**, *498*, 192−197.
(30) Sablon, N.; De Proft, F.; Ayers, P. W.; Geerlings, P. *J. Chem. Theory Comput.* **2010**, *6*, 3671−3680.
(31) Sablon, N.; De Proft, F.; Sola, M.; Geerlings, P. *Phys. Chem. Chem. Phys.* **2012**, *14*, 3960−3967.
(32) Fias, S.; Geerlings, P.; Ayers, P. W.; De Proft, F. *Phys. Chem. Chem. Phys.* 2013; DOI: 10.10391/c2ep43612d.
(33) Cioslowski, J.; Martinov, M. *J. Chem. Phys.* **1994**, *101*, 366−370.
(34) Torrent-Sucarrat, M.; Salvador, P.; Geerlings, P.; Solà, M. *J. Comput. Chem.* **2007**, *28*, 574−583.
(35) Torrent-Sucarrat, M.; Salvador, P.; Solà, M.; Geerlings, P. *J. Comput. Chem.* **2008**, *29*, 1064−1072.
(36) Savin, A.; Colonna, F.; Allavena, M. *J. Chem. Phys.* **2001**, *115*, 6827−6833.
(37) (a) Sperber, G. *Int. J. Quantum Chem.* **1971**, *5*, 189−214. (b) Lassettre, E. N. *J. Chem. Phys.* **1985**, *83*, 1709−1721. (c) Parr, R. G.; Rupnik, K.; Ghosh, S. K. *Phys. Rev. Lett.* **1986**, *56*, 1555−1558. (d) Hunter, G. *Int. J. Quantum Chem.* **1986**, *29*, 197−204. (e) Sagar, R. P.; Ku, A. C. T. *Can. J. Chem.—Rev. Can. Chim.* **1988**, *66*, 1005−1012. (f) Sagar, R. P.; Ku, A. C. T.; Vedene H. Smith, J.; Simas, A. M. *J. Chem. Phys.* **1988**, *88*, 4367−4374. (g) Becke, A. D.; Edgecombe, K. E. *J. Chem. Phys.* **1990**, *92*, 5397−5403. (h) Levit, C.; Sarfatti, J. *Chem. Phys. Lett.* **1997**, *281*, 157−160. (i) Kohout, M. *Int. J. Quantum Chem.* **2001**, *83*, 324−331. (j) Schmider, H. L.; Becke, A. D. *J. Chem. Phys.* **2002**, *116*, 3184−3193. (k) Ayers, P. W.; Parr, R. G.; Nagy, A. *Int. J. Quantum Chem.* **2002**, *90*, 309−326. (l) Ayers, P. A. *J. Chem. Sci.* **2005**, *117*, 441−454. (m) Bohórquez, H. J.; Boyd, R. J. *J. Chem. Phys.* **2008**, *129*, 024110. (n) Ángyán, J. G. *Int. J. Quantum Chem.* **2009**, *109*, 2340−2347. (o) Bohorquez, H. J.; Boyd, R. J. *Theor. Chem. Acc.* **2010**, *127*, 393−400. (p) Rincon, L.; Alvarellos, J. E.; Almeida, R. *Phys. Chem. Chem. Phys.* **2011**, *13*, 9498−9506.
(38) Ayers, P. W.; Anderson, J. S. M.; Bartolotti, L. J. *Int. J. Quantum Chem.* **2005**, *101*, 520−534.
(39) Fievez, T.; Sablon, N.; De Proft, F.; Ayers, P. W.; Geerlings, P. *J. Chem. Theory Comput.* **2008**, *4*, 1065−1072.
(40) Ayers, P. W. *Faraday Discuss.* **2007**, *135*, 161−190.
(41) Hehre, W. J.; Radom, L.; Schleyer, P. V. R.; Pople, J. *Ab Initio Molecular Orbital Theory*; Wiley: New York, 1986.
(42) Kendall, R. A.; Thom H. Dunning, J.; Harrison, R. J. *J. Chem. Phys.* **1992**, *96*, 6796−6806.
(43) Woon, D. E.; Dunning, T. H. J. *J. Chem. Phys.* **1993**, *98*, 1358−1371.
(44) Wilson, A. K.; Woon, D. E.; Peterson, K. A.; Dunning, T. H. J. *J. Chem. Phys.* **1999**, *110*, 7667−7676.
(45) Perdew, J. P.; Burke, K.; Ernzerhof, M. *Phys. Rev. Lett.* **1996**, *77*, 3865−3868.
(46) Rousseau, B.; Peeters, A.; Van Alsenoy, C. *Chem. Phys. Lett.* **2000**, *324*, 189−194.
(47) Frisch, M. J.; Trucks, G. W.; Schlegel, H. B.; Scuseria, G. E.; Robb, M. A.; Cheeseman, J. R.; Scalmani, G.; Barone, V.; Mennucci, B.; Petersson, G. A.; Nakatsuji, H.; Caricato, M.; Li, X.; Hratchian, H. P.; Izmaylov, A. F.; Bloino, J.; Zheng, G.; Sonnenberg, J. L.; Hada, M.; Ehara, M.; Toyota, K.; Fukuda, R.; Hasegawa, J.; Ishida, M.; Nakajima, T.; Honda, Y.; Kitao, O.; Nakai, H.; Vreven, T.; Montgomery, J. A., Jr.; Peralta, J. E.; Ogliaro, F.; Bearpark, M.; Heyd, J. J.; Brothers, E.; Kudin, K. N.; Staroverov, V. N.; Kobayashi, R.; Normand, J.; Raghavachari, K.; Rendell, A.; Burant, J. C.; Iyengar, S. S.; Tomasi, J.; Cossi, M.; Rega, N.; Millam, J. M.; Klene, M.; Knox, J. E.; Cross, J. B.; Bakken, V.; Adamo, C.; Jaramillo, J.; Gomperts, R.; Stratmann, R. E.; Yazyev, O.; Austin, A. J.; Cammi, R.; Pomelli, C.; Ochterski, J. W.; Martin, R. L.; Morokuma, K.; Zakrzewski, V. G.; Voth, G. A.; Salvador, P.; Dannenberg, J. J.; Dapprich, S.; Daniels, A. D.; Farkas, Ö; Foresman, J. B.; Ortiz, J. V.; Cioslowski, J.; Fox, D. J. *Gaussian 09*, revision A.1; Gaussian Inc.: Wallingford, CT, 2009.
(48) Murray, C. W.; Handy, N. C.; Laming, G. J. *Mol. Phys.* **1993**, *78*, 997−1014.
(49) Lebedev, V. I.; Skorokhodov, A. L. *Russ. Acad. Sci. Doklady Math.* **1992**, *45*, 587−592.
(50) Gill, P. M.; Johnson, B. G.; Pople, J. A. *Chem. Phys. Lett.* **1993**, *209*, 506−512.
(51) Langenaeker, W.; Liu, S. *J. Mol. Struct.: THEOCHEM* **2001**, *535*, 279−286.
(52) Politzer, P. *J. Chem. Phys.* **1980**, *72*, 3027−3033.
(53) Kakkar, M.; Sen, K. D. *Chem. Phys. Lett.* **1994**, *226*, 241−244.
(54) De Proft, F.; Sen, K. D.; Geerlings, P. *Chem. Phys. Lett.* **1995**, *247*, 154−158.
(55) Atkins, P.; Jones, L. *Chemical Principles*; W. H. Freeman: New York, 2006; pp 582−583.
(56) Mitroy, J.; Safronova, M. S.; Clark, C. W. *J. Phys. B: At., Mol., Opt. Phys.* **2010**, *43*, 202001.